Journal of Applied Polymer Science

Toughness Optimization of Elastomer-Modified Glass-Fiber Reinforced PA6 Materials

Markus Kroll,[1] Beate Langer,[2] Wolfgang Grellmann[2,3]
[1]BASF Leuna GmbH, Leuna D-06237, Germany
[2]Polymer Service GmbH Merseburg, Merseburg D-06217, Germany
[3]Martin-Luther University Halle-Wittenberg, Center of Engineering Sciences, Halle/Saale D-06099, Germany
Correspondence to: M. Kroll (E-mail: markus.kroll@basf.com)

ABSTRACT: To investigate the influence of moisture and EPR-*g*-MA content on the fracture behavior of glass–fiber reinforced PA6 materials, brittle-to-tough transition temperatures (T_{btt}) were determined. Water absorption was taken into account by conditioning the analyzed materials. Tensile tests could reveal the temperature range of the largest moisture dependence of mechanical properties between 10 and 50°C. *J*-integral values were used to describe the fracture behavior under conditions of impact load as a function of temperature. The brittle-to-tough transition of reinforced polyamides was found to be less approximate than in unreinforced materials. Two different characteristic temperature points T_s and T_e were identified, which were the intercept between elastic and elastic–plastic deformation on the one hand and the starting point of dominating stable crack propagation with strong plastic deformation on the other hand. Characteristic brittle-to-tough transition temperatures T_{btt} could be calculated as the arithmetic average of these two points. © 2012 Wiley Periodicals, Inc. J. Appl. Polym. Sci. 000: 000–000, 2012

KEYWORDS: brittle-to-tough transition; glass-fibers; *J*-integral; PA6 elastomer blends

Received 27 June 2011; accepted 18 January 2012; published online
DOI: 10.1002/app.36853

INTRODUCTION

Today polyamide materials are commercially available in a vast variety of compositions and modifications. The inclusion of rigid components of different aspect ratios (e.g., particles, fibers, and sheets) and various size scales as well as rubber components are used to customize mechanical properties among others.

Glass–fiber reinforced polyamide 6 (PA6)/elastomer blends have been subject of several publications concerning rheological, thermal, and especially mechanical properties.[1–12] The toughness of polyamide materials is temperature dependent. Characteristic brittle-to-tough transition temperatures (T_{btt}) have been identified of several PA6 compounds containing glass–fibers or blend components or both.[10,11,13–18] The brittle-to-tough transition of neat PA6 occurs at 75°C on impact loading in the instrumented Charpy impact test (ICIT).[19] Water absorption leads to a decrease of T_{btt} in neat PA6 to lower temperatures. These characteristic temperatures were found to be 40°C in case of normal conditioning and about −20°C in case of water storage.[20] The value of T_{btt} ranges from −40 to 40°C for unreinforced modified PA6 materials containing EPR-*g*-MA, SEBS-*g*-MA, BA or other elastomers.[11,15,19,20] It is well known that rise of elastomer content or concentration of compatibilizing agents as well as reduction of modifier particle size increase toughness and shift T_{btt} to lower temperatures.[10,11,14,15,19] Conversely, increasing the fiber content of toughened polyamides leads to diminishing of sharp toughness shift and promotes a more gradual toughness decline if temperature is lowered.[11]

As the named publications focused on the properties of PA6/elastomer blends with glass–fiber inclusion as a method to enhance their properties,[1–18] there is a lack of information concerning the toughness behavior of PA6 materials with high glass–fiber contents. Therefore this study aims on the optimization of material properties of glass–fiber reinforced PA6 compounds using EPR-*g*-MA addition as a toughness enhancement strategy. PA6 materials with 40, 50 wt % or even higher amounts of glass–fibers are used for functional parts that are exposed to very high mechanical loads. Here toughness is not a main criterion of material development but has to be optimized to fit the demands of fast and secure manufacturing and to avoid brittle fracture in the range of application conditions like temperature, moisture, and loading speed.

EXPERIMENTAL

Materials

Elastomer-modified PA6 glass–fiber compounds were produced on a corotating twin screw extrusion machine. The commercial PA6 grade ULTRAMID® B27 E supplied by BASF SE

Table I. Composition and Material Properties

PA6 (wt %)	EPR-g-MA (wt %)	Blend ratio	Water content		Tensile test at 23°C		
			Compound (wt %)	PA6 phase (wt %)	E_t (GPa)	σ_m (MPa)	ε_B (%)
PA6/E GF40 dry (d)							
59	0	100/0	<0.05	<0.1	12.8	219	3.9
54	5	92/8			11.9	193	4.0
51.5	7.5	87/13			11.4	181	4.1
49	10	83/17			11.0	169	4.5
PA6/E GF40 conditioned (c)							
59	0	100/0	1.78	3.02	8.6	144	6.9
54	5	92/8	1.62	3.01	7.9	132	8.0
49	10	83/17	1.44	2.95	7.2	121	9.3

(Ludwigshafen, Germany) was used as the matrix polymer. Each analyzed material was colored black by use of carbon black masterbatch. The influence of carbon black on the fracture behavior of glass–fiber reinforced PA6/PA66 blends had been investigated before.[21,22] After drying granulates at 80°C for 24 h in a condensation dryer, the specimens were injection molded. The materials were mechanically tested in dry and conditioned state. Conditioning was done at 62% relative humidity and 70°C until the moisture equilibrium had established according to ISO 1110.[23] Subsequently, conditioned specimens had been stored in a conditioned laboratory (23°C, 50% r.h.) where the testing later took place, dry specimens were stored in a desiccator with silica gel until testing. The total moisture absorptions of the materials were measured gravimetrically and thereby the moisture contents of the PA6 could be calculated. Tensile tests were performed according to ISO 527[24] at normal climate. The composition of each of the materials of this study together with the moisture absorption and some mechanical properties are shown in Table I.

While modulus and tensile strength are decreasing with rising elastomer content, elongation at break is increasing both dry and conditioned. Moisture absorption reduces strength and stiffness on 65–70% of the values in the dry materials whereas elongation at break is doubled. Because of the high amount of fiber reinforcement necking occurred in no material.

Temperature Dependent Mechanical Behavior

Besides the testing at normal climate, static tensile tests according to ISO 527[24] were performed on an Instron testing machine with a climate chamber in the temperature range between 0 and 80°C. Specimens were placed in the climate chamber for 30 min to assure constant temperature conditions.

Temperature Dependent Toughness Behavior

To get a profound knowledge about the temperature dependent fracture behavior under impact, load-deflection diagrams (*F-f* diagram) were recorded and analyzed at several temperatures using the instrumented Charpy impact test (ICIT). Thereby brittle-to-tough transition temperatures could be identified. An example of a load-deflection diagram is illustrated in Figure 1. It represents a load-deflection (*F–f*) diagram with elastic–plastic behavior of Type II according to the classification of Grellmann and Seidler.[25] It is characterized by the transition from elastic to elastic–plastic material behavior at the point (F_{gy}, f_{gy}). The consumed energy can be graphically separated in an elastic part A_{el} and a plastic part A_{pl}.

The experimental procedure and the testing conditions followed strictly the "procedure for determining the crack resistance behavior by ICIT."[26] Single edge notched bend (SENB) specimens with the dimensions 4 × 10 × 80 mm^3 ($B \times W \times L$) were tested in this study. For each load condition, 10 specimens were tested. For the characterization of the unstable crack growth behavior, the initial crack a had a length of 2 mm resulting in an a/W ratio of 0.2 and was cut with a razor blade. The characteristic value J_{Id} was calculated according to the *J*-integral estimation method of SUMPTER and TURNER given in eq. (1), where both the elastic energy share A_{el} and the plastic energy share A_{pl} are implicated.

$$J_{Id}^{ST} = \eta_{el}\frac{A_{el}}{B(W-a)} + \eta_{pl}\frac{A_{pl}}{B(W-a)}\frac{W-a_{eff}}{W-a} \quad (1)$$

The notch depth influence is represented by the geometric functions η_{el} of eq. (2) and η_{pl} of eq. (3) and the effective crack length by a_{eff}.[26]

$$\eta_{el} = \frac{2F_{gy}s^2(W-a)}{f_{gy}E_dBW^3}f^2(a/W)(1-\nu^2) \quad (2)$$

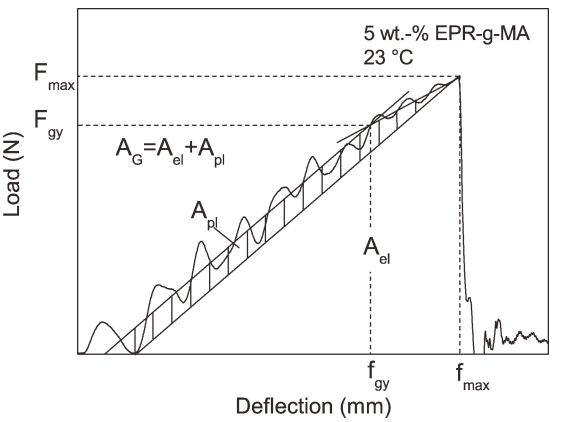

Figure 1. Illustration example of a typical load-deflection diagram of PA6/E GF40 dry; the total amount of consumed energy A_G can be separated in A_{el} and A_{pl}.

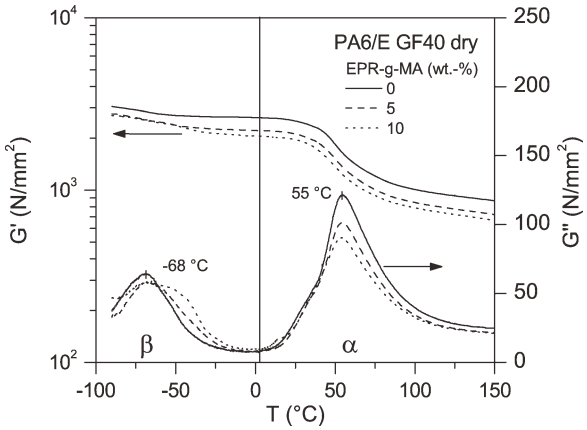

Figure 2. Storage and loss modulus of dry materials.

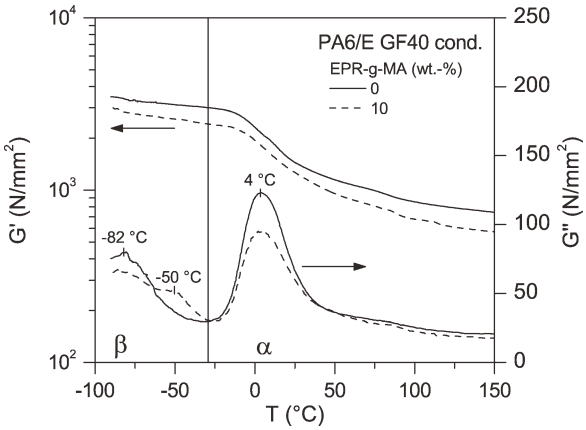

Figure 3. Storage and loss modulus of conditioned materials.

$$\eta_{pl} = 2 - \frac{(1 - a/W)(0.892 - 4.476a/W)}{1.125 + 0.892a/W - 2.238(a/W)^2} \quad (3)$$

RESULTS AND DISCUSSION

Effect of Moisture on Viscoelastic Properties

Moisture in polyamides is decreasing the glass transition temperature. To characterize this effect, T_g has been determined by dynamic mechanical analysis as the maximum of the loss modulus according to ISO 6721-1[27] (Figures 2 and 3). Glass transition temperatures in the unmodified materials were $T_g^{PA6d} = 55°C$ in dry state and $T_g^{PA6c} = 4°C$ in conditioned state.

The location of the peak glass transition temperature is independent of the elastomer content (Figure 2). The β transition as the temperature range of chain segment and amid group movements on the one hand and the α transition as main glass transition temperature range with chain segment movement initiation within the amorphous phase[28] are located at -68 and $55°C$ in the dry materials. The onset of glass transition can be identified in the temperature range between 0 and 25°C.

Only the peak height was influenced by the EPR-*g*-MA/PA6 ratio. Beside the peak height influence, there is an overlap of the β transition peak at $-68°C$ and the peak glass transition temperature of the elastomer phase. In Figure 4, both effects are separated by subtracting the loss modulus curve of the 10 wt % elastomer-modified material from the unmodified material. The peak glass transition of the EPR-*g*-MA was thereby identified at $-43°C$.

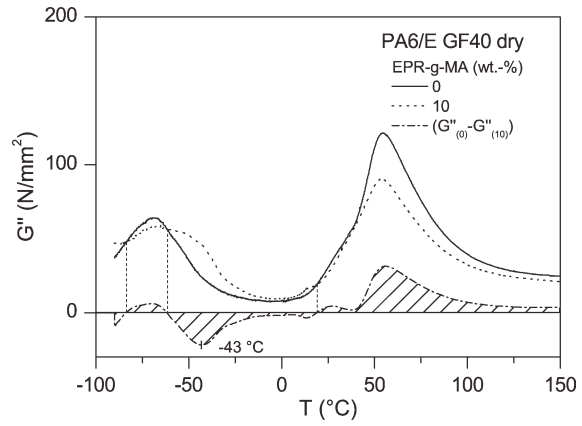

Figure 4. Identification of elastomer phase peak glass transition temperature.

Conditioning shifts the transition temperature range towards lower temperatures of $-82°C$ in case of the β transition and $4°C$ in case of α transition (Figure 3).

Behavior Under Quasi-Static Load

Elastic modulus and tensile strength as functions of temperature and elastomer content are illustrated in Figures 5 and 6 both dry and conditioned. The modulus of dry materials is decreasing with maximum slope of the $E_t - T$ curve between 40 and 60°C (Figure 5) in a convex shape. Conditioning shifts the modulus curves towards lower temperatures and is resulting in a concave shape in the analyzed temperature range.

The maximum tensile strength in Figure 6 is decreasing more continuously. The slope maxima of Young's modulus and maximum tensile strength are arranged in the adjacent area of glass transition temperatures.

The unmodified glass–fiber reinforced material provides a high level of strength and stiffness. Elastomer modification of 10 wt % EPR-*g*-MA leads to a loss of about 15–25% of these mechanical properties in the whole temperature range and in both moisture conditions. Elongation at break in Figure 7 is strongly dependent on water content as well. Even a 10 wt % elastomer-modified dry compound does not achieve the same level of elongation at break as the unmodified material after water absorption within the temperature range from 10 to 50°C. The importance of property changes of polyamides induced by water absorption was intensively discussed before[29–34] and is of special interest in consideration of the temperature range with the greatest property difference between dry and conditioned material state. This range is located between 10 and 50°C and is corresponding to the temperatures of the glass transitions of dry and conditioned materials. Figure 8 illustrates that the relative tensile properties of the conditioned materials drop to 50% of the dry material in this range.

Applied Polymer SCIENCE

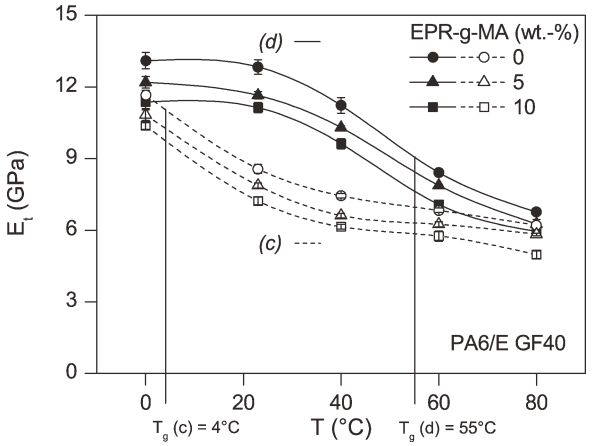

Figure 5. Young's modulus of dry and conditioned materials.

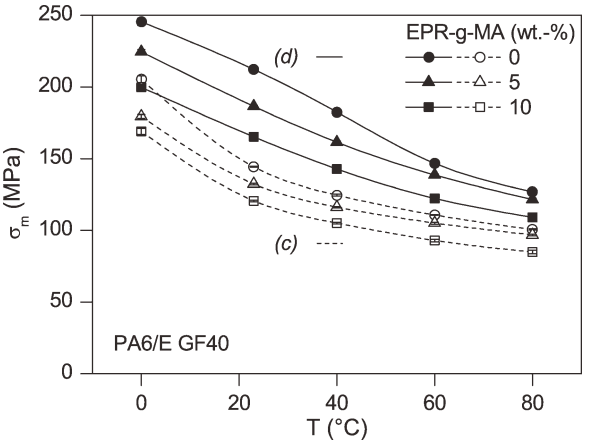

Figure 6. Tensile strength as a function of temperature.

Toughness Behavior Under Impact Load

Influence of Testing Temperature. Toughness of analyzed materials is strongly temperature dependent. Figure 9 illustrates the change of load-deflection diagrams of a dry 5 wt % EPR-*g*-MA-modified PA6 GF40 material while temperature increases. Higher temperatures raise the amount of plastic deformation. At -40°C the load-deflection curve represents linear-elastic material behavior.

At 23°C, beyond the glass transition temperature of dry PA6, the behavior is elastic–plastic with F_{gy} as a characteristic point of the curve. However, unstable crack propagation still occurs at this temperature. Rising matrix ductility above T_g (55°C, see also Figure 2) is responsible for the dominant stable crack propagation at 60°C. There the crack is arrested because of the raising amount of energy consumption during crack propagation, which is represented by the value A_R. Maximum load and the corresponding deflection are functions of temperature with different progressions. Figure 10 shows both characteristics of the fracture process of dry 5 wt % EPR-*g*-MA-modified PA6 GF40. There are strong correlations between these two values and characteristic temperatures of DMA temperatures. The maximum load is increasing with the highest slope between $T_g^{\text{EPR-}g\text{-MA}}$ and the onset of PA6 glass transition. This can be interpreted as an enhancement of the toughening mechanism of elastomer particles, which become more ductile whereas the PA6 still exists as a stiff matrix. F_{max} has its peak exactly within the range of PA6 T_g onset. From this point, F_{max} is decreasing monotonously. At the same time, the existence of F_{gy} from 0°C indicates that brittle fracture is only apparent at temperatures lower than 0°C. Starting from $T_g^{\text{EPR-}g\text{-MA}}$ the corresponding deflection f_{max} is increasing strongly in a linear way. At T_g^{PA6} temperature the slope of the temperature-deflection curve is exponentially rising, indicating large deformations before fracture that arise from the matrix plastification above T_g^{PA6}.

This temperature dependence of the deformation and crack propagation behavior can be described with the *J*-integral value. The parameter J_i is defined by energy dissipation during fracture process and therefore is including both the load and the deformation as determining influences of the fracture process. Figure 11 shows the temperature dependence of J_{Id} of dry 5 wt % EPR-*g*-MA-modified PA6 GF40.

The parameter J_{Id} is strongly increasing with rising temperature. The values of J_{Id} beyond the onset temperature range of PA6 at 0°C can be fitted exactly by a linear regression. At a certain

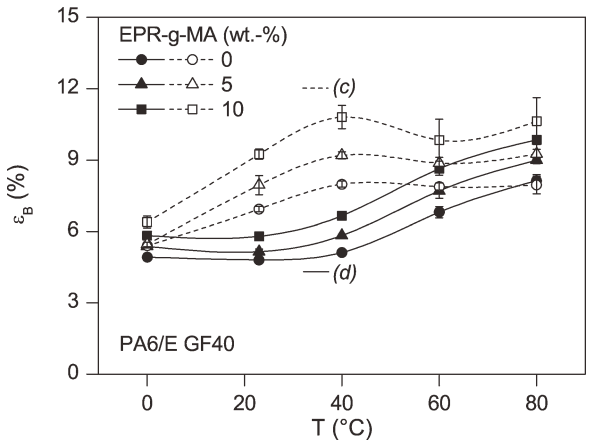

Figure 7. Elongation at break as a function of temperature.

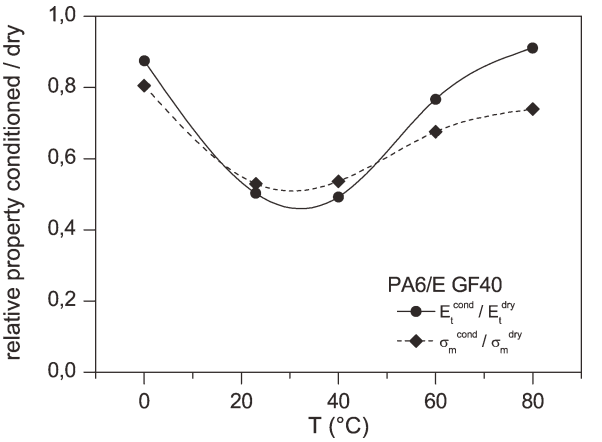

Figure 8. Influence of water conditioning on stiffness and strength, represented by the quotient of the values of the conditioned material and the dry material.

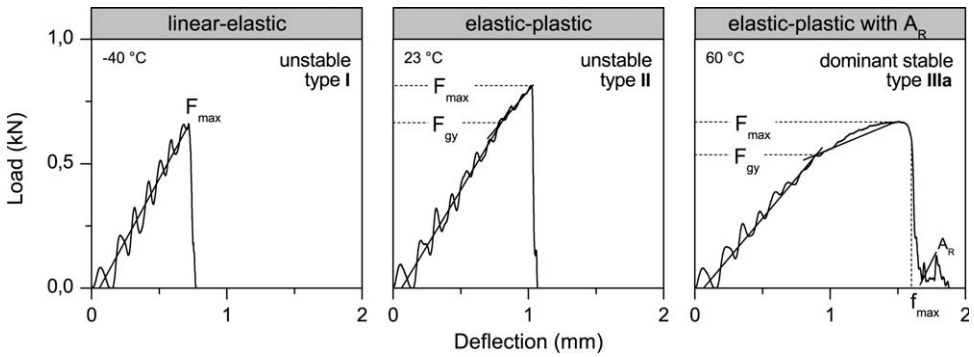

Figure 9. Load-deflection curves from instrumented Charpy impact test at different temperatures of dry 5 wt % EPR-*g*-MA-modified PA6 GF40; diagram types are defined according to Grellmann and Seidler.[25]

temperature, the toughness behavior changes, indicated by a higher slope of the $T - J_{Id}$ curve. This corresponds with the existence of a brittle-to-tough transition temperature in unreinforced and low reinforced elastomer-modified PA6 compounds, as reported by other authors.[11,15,19,20] The used modifier together with the included glass–fibers are responsible for a smooth toughness change as it was observed in reinforced PA6 by measurement of the Izod impact toughness by Laura et.al.[11]

At −40°C, there is no significant matrix deformation during fracture [Figure 12(a)]. Main energy consuming phenomena are fiber pullout as well as brittle fracture of the matrix material between fibers. At 0°C, the matrix regions of the fracture surface look smoother, indicating greater matrix ductility [Figure 12(b)]. Further on more adhered matrix material is found on the fibers. Fibers are not pulled out as cleanly as they were at −40°C which is one explanation for the significant load increase in Figure 10.

Above this point, the shape of the curve is changing as well as the matrix deformation, which is characterized by large amounts of shearing and even the building of fibrillae [Figure 12(c)]. Zero-degree Celsius is the initial temperature of F_{gy} appearance and the corresponding load-deflection diagram Type II. From there J_{Id} is increasing linearly with a raised slope. Each of the analyzed materials was characterized by a bifid linear J_{Id} function of temperature.

Brittle-to-Tough Transition Temperature Calculation. The analysis of J_{Id} as a function of temperature allows a characterization of brittle-to-tough transition by separating the curve in sections with different slopes as described above. Therefore, three basic toughness behavior sections I–III have been identified for each material. The construction principle is illustrated for the unmodified conditioned compound in Figure 13.

Complete brittle behavior without any yielding was apparent in Section I with the corresponding diagram Type I. The lower toughness level was defined by a linear approximation in this section. In Section II, dominating unstable crack propagation is found with a raising portion of yielding and plastic deformation and diagram Type II, respectively. The points of this section were fitted by a linear regression too. The intersection of the two lines of Sections I and II defines the starting temperature T_s of the brittle-to-tough transition range. The upper toughness Section III is defined by the last temperature where unstable crack propagation was the dominating process. Above this temperature, the stable crack propagation occurred without complete specimen breakage. The J_{Id} concept of elastic–plastic fracture mechanics becomes invalid in case of dominant stable

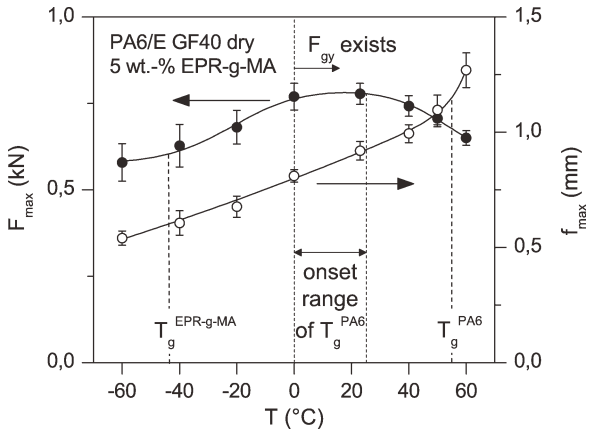

Figure 10. Maximum load and corresponding deflection as a function of temperature in dry 5 wt % modified PA6 GF40.

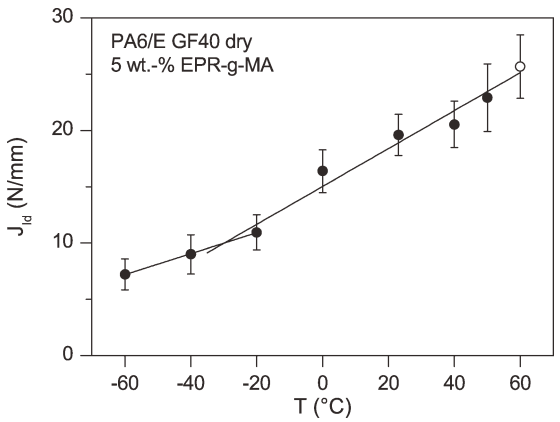

Figure 11. J_{Id} as a function of temperature for dry 5 wt % EPR-*g*-MA-modified PA6 GF40 (● dominant unstable, ○ dominant stable).

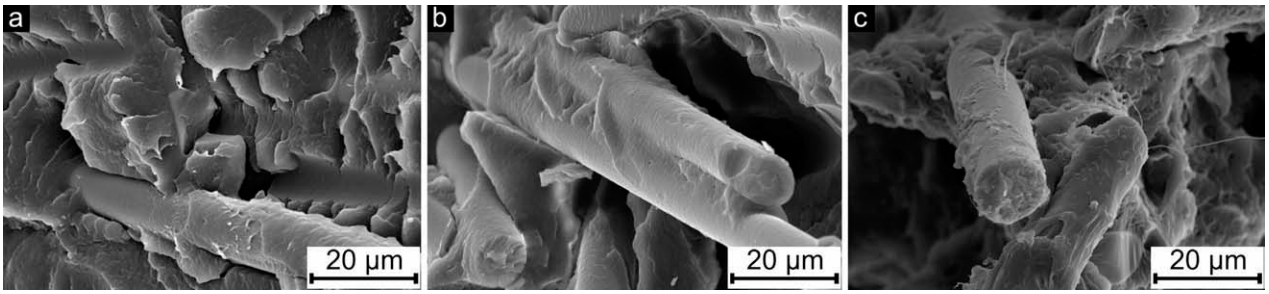

Figure 12. Fracture surfaces of dry PA6 materials with 5 wt % elastomer content at different temperatures: (a) −40°C, (b) 0°C, and (c) 23°C.

crack propagation. The determination of crack initiation values of J_{Id} at F_{max} is still possible at higher temperatures; but this value would only characterize crack initiation and would neglect crack propagation energies that lead to higher toughness. Therefore, it is not comparable with the values at lower temperatures were the whole energy consumption is part of the calculation. Therefore the transition point between elastic plastic deformation with small scale yielding and dominating stable crack propagation T_e is marked as the average between the last temperature of Section II and the first temperature with stable crack propagation.

T_{btt}, thereby, could easily be determined as the temperature which separates the resulting segment line $\overline{T_s T_e}$ in two equal parts. This calculation is similar to the method of lower and upper shelf of toughness that proved to be efficient for the characterization of T_{btt} of neat PA6[35] and PA6/BA blends[19] and was originally invented for metals.[36] But especially, the lower shelf is characterized by a nearly constant temperature independent J_{Id} value. In case of EPR-*g*-MA-modified PA6 glass–fiber materials, J_{Id} proved to be linearly dependent on the temperature in the brittle region too. Therefore the bifid linear approximation as a method to calculate T_{btt} has to be used to give accurate values of T_{btt}.

Influence of Elastomer Content. Elastomer modification of PA leads to a multiple shear yielding process, as the main toughness increasing mechanism which initially appears above T_g of the elastomer phase.[37] This is also the case in reinforced materials of this study. Both dry and conditioned they reveal a rising toughness dependence of modifier content above −60°C (Table II), the highest slope of F_{max} in Figure 10 can also be linked to the beginning of multiple shear yielding in a PA6 matrix of high strength and stiffness.

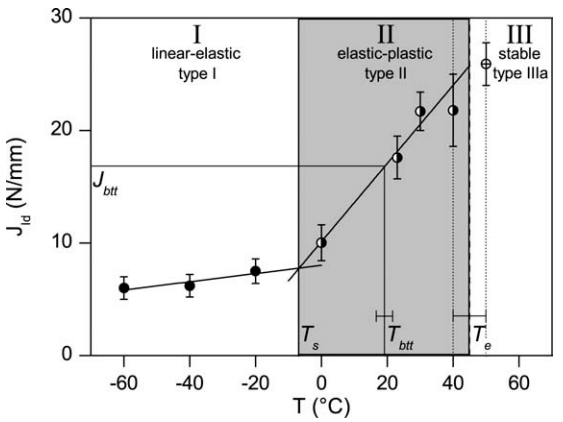

Figure 13. Determination of T_{btt} by linear toughness approximation in different deformation behavior sections for conditioned unmodified PA6 GF40.

Figure 14 shows the J_{Id} values as a function of elastomer content for three different temperatures. At each testing temperature, the elastomer-modified materials provide a higher toughness than the unmodified PA6 GF40. At 23°C, there is hardly any difference between the toughness of the materials of different EPR-*g*-MA content.

In Figure 15, the fracture surfaces of these dry materials are illustrated. It becomes obvious that the unmodified material is still represented by a very brittle fracture with low matrix shearing in the fiber surrounding at 23°C [Figure 15(a,d)]. Even if the fracture overview indicates a stronger matrix plastification

Table II. J_{Id} Values at Different Temperatures and Moisture Conditions

	J_{Id} dry (N/mm)			J_{Id} conditioned (N/mm)		
	EPR-*g*-MA content (wt %)			EPR-*g*-MA content (wt %)		
T (°C)	0	5	10	0	5	10
−60	6.4	7.2	8.2	6	6.5	6.7
−40	7.5	8.9	12.9	6.2	7.8	10.5
−20	8.2	10.9	17.5	7.5	8.9	13.7
0	9.8	16.4	19.4	10.0	14.9	17.1
10	-	-	-	-	17.4	19.6
23	14.2	19.6	19.8	17.6	21.7	25.5
30	-	-	20.8	21.7	23.8	
40	16.6	20.5	20.6	21.8		
50	-	22.9		25.9		
60	20.1	25.6				
70	21.3					
85	21.6					

Light gray shades represents diagram Type I, white shades represents diagram Type II, and dark gray shades represents diagram Type IIIa.

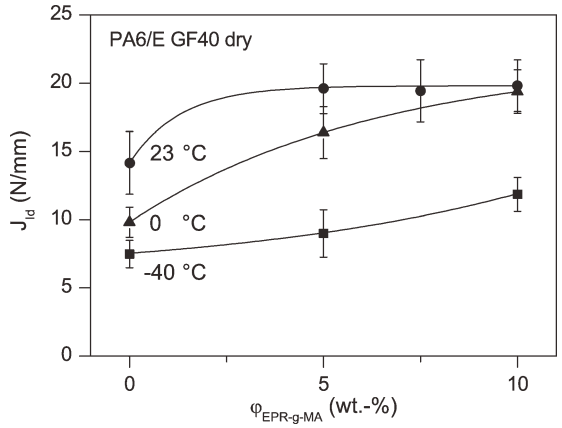

Figure 14. J_{Id} as a function of elastomer content.

and deformation in 10 wt % EPR-*g*-MA [Figure 15(c)], shearing and the amount of adhered matrix material on fibers are similar to the material with half the elastomer content [Figure 15(e,f)]. In Table II, J_{Id} values of each material are listed at different testing temperatures.

The toughness rise caused by elastomer modification reaches its maximum at 0°C, both dry and conditioned with relative J_{Id} increases of 98% (dry) and 82% (conditioned). Most of the materials show the same bifid slope behavior as discussed above.

Only the dry 10 wt % EPR-*g*-MA-modified material is characterized by a different behavior. Here, J_{Id} is increasing with the highest slope between −60 and 0°C. Above 0°C, the toughness is stagnating at about 20 N/mm. The high amount of added elastomer leads to a load increase at even lower temperatures than in case of addition of 5 wt % EPR-*g*-MA (Figure 16 compared to Figure 10).

Figure 16 clearly indicates that the load is decreasing from 0°C, but as a difference to the behavior of the material with 5 wt % (Figure 10), the deflection does not increase linearly from this point but with a decreasing slope. J_{Id} is influenced by load and deformation. Therefore the load decrease cannot be compensated by raised deformation and deflection in the case of the highest analyzed elastomer content with the result of a stagnating J_{Id} above 0°C.

This is the only analyzed material whose maximal J_{Id} value is located within the temperature range of elastic–plastic behavior and not at the end of it. To get comparable T_{btt} values, T_s was defined at -60°C and T_e at the end of J_{Id} increase at 0 C in this case.

Influence of Moisture. Moisture absorption delays the glass transition temperature towards lower temperatures. Without elastomer modification, this leads to enhancement of J_{Id} values in the range of elastic–plastic material behavior above 0°C in Figure 17. Here the rise of matrix ductility of the conditioned material provides higher toughness.

Stable crack propagation begins at 20–30°C lower temperatures after water absorption in any material. Another parallelism between unmodified and elastomer-modified materials is the moisture-induced toughness reduction below the beginning temperature of elastic plastic material behavior (Table II). During moisture absorption, water molecules are mainly introducing the amorphous regions of polyamides,[34] at the same time crystalline regions are affected as well but only to a very moderate extent.[38,39] The enhanced ductility after conditioning is responsible for early beginning of stable crack propagation and raised toughness of unmodified material in Figure 17.

Figure 18 illustrates the changes in deformation behavior on the fracture surfaces. Compared to the fracture surfaces of the dry material (Figure 12), the induced moisture establishes a large

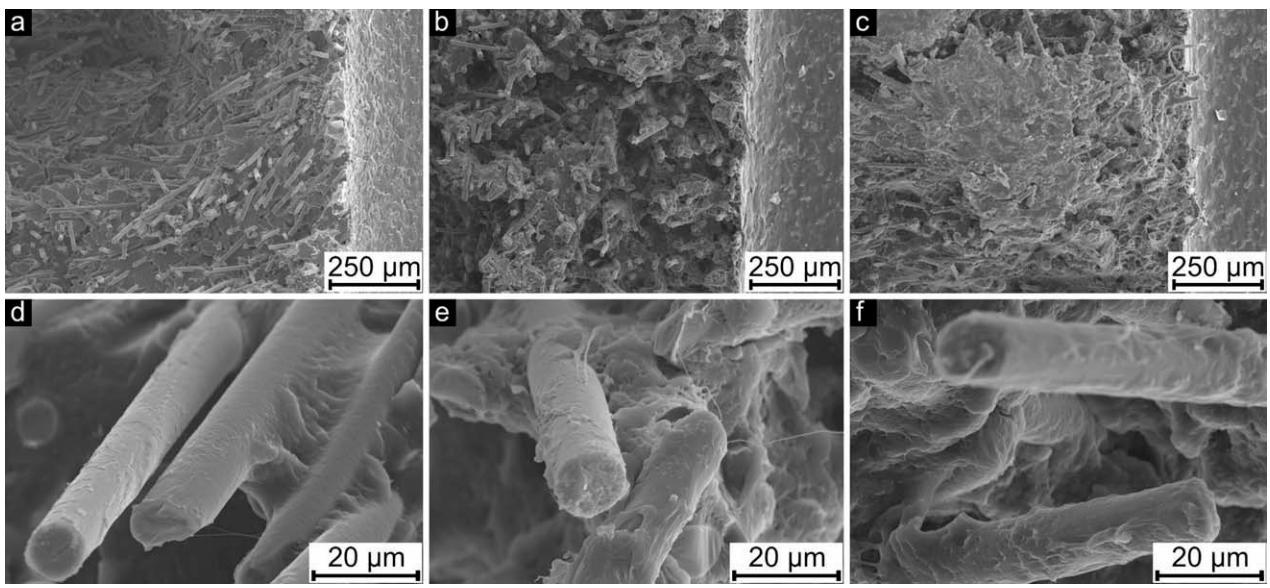

Figure 15. Fracture surfaces of dry PA6 compounds at 23°C with different contents of EPR-*g*-MA: (a,d) 0 wt %, (b,e) 5 wt %, and (c,f) 10 wt %.

Applied Polymer SCIENCE

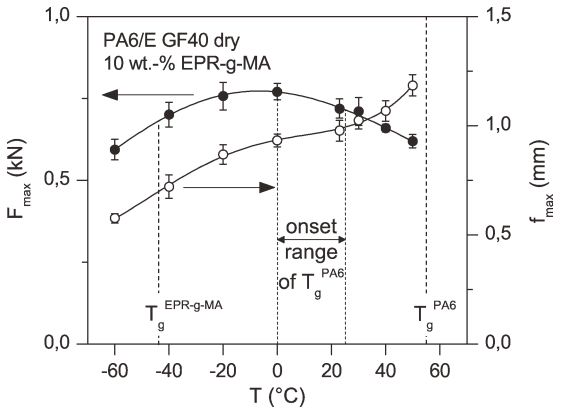

Figure 16. Maximum load and corresponding deflection as a function of temperature in dry 10 wt % modified PA6 GF40.

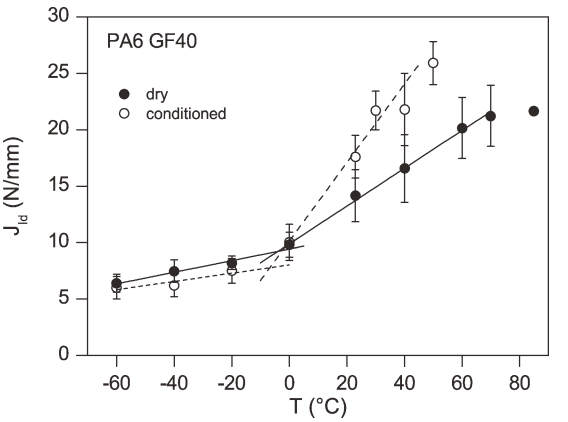

Figure 17. Effect of water absorption on the J_{Id} values of unmodified PA6 GF40.

amount of cavities at 0 and 23°C. At the same time, water leads to toughness reduction at temperatures with elastic material behavior and brittle fracture in any material. Water conditioning leads to a reduction of J_{Id} of the modified materials in the temperature range up to 10°C (Table II).

Modification of highly reinforced polyamides with small amounts of elastomer is used to improve the resistance of the material against brittle fracture on the one hand, but also to provide toughness properties of conditioned materials in dry state directly from injection molding on the other hand. This is important to assure fast and safe finishing or assembly of parts with clip and plug connections without introducing material failures that in use could lead to fracture. Therefore, moisture induced toughness reduction in the analyzed modified reinforced materials that emerges up to 0–10°C has to be considered. In this temperature range, moisture absorption is crucial because it decreases stiffness, strength, and resistance against unstable crack propagation.

Toughness Optimization. The toughness was found to be dependent on elastomer content, moisture, and testing temperature. As J_{Id} is a fracture mechanics parameter that values the amount of energy dissipation during crack propagation, each of the three influence factors significantly enhances matrix deformation and leads to raising amounts of sheared matrix material, adhered matrix on fiber surfaces, and more fiber pullout with matrix yielding than simple pullout of smooth fibers without matrix deformation (Figures 12, 15, and 18).

Rising elastomer content decreases the brittle-to-tough transition temperature both dry and conditioned (Figure 19). In case of dry fiber reinforced PA6 materials, T_{btt} declines from 37 to −30°C by addition of 10 wt % EPR-*g*-MA. T_{btt} decreases from about 19°C for PA6 GF40 to -22°C in the conditioned materials. That means elastomer modification leads to a brittle-to-tough transition at lower temperatures as well as moisture conditioning in case of unmodified and 5 wt % EPR-*g*-MA-modified 40 wt % glass–fiber reinforced materials. Therefore, high toughness and stable crack propagation is achieved earlier. However, toughness in the transition section does not reveal an identical dependence. Therefore, the temperature T_{btt} cannot be used as a single optimization criterion. To get a quick impression of the toughness behavior, Figure 20 illustrates temperatures of equal toughness compared to the unmodified dry material at room temperature. This shows that modification with 10 wt % EPR-*g*-MA endows the material with room temperature toughness of a dry unmodified material at -30°C. Conditioned room temperature toughness is not reached until -21°C, which is contrary to the overall moisture induced ductility increase.

CONCLUSION

The mechanical properties of elastomer-modified 40 wt % glass–fiber reinforced materials appeared strongly dependent on modifier content, absorbed moisture, and temperature. Moisture

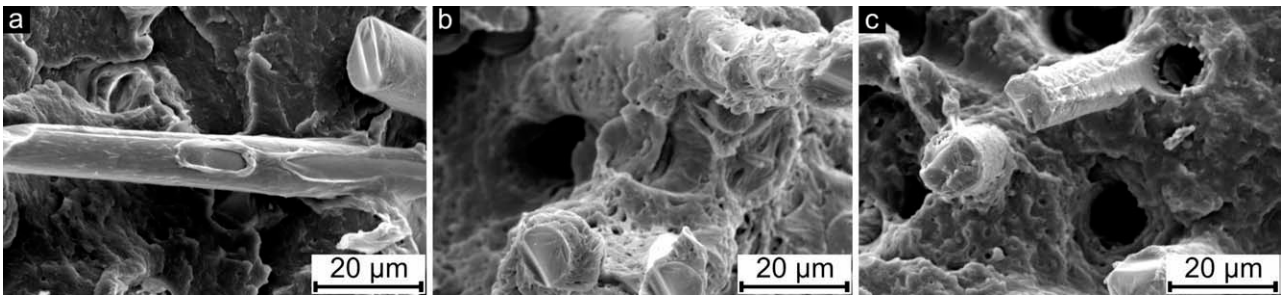

Figure 18. Fracture surfaces of conditioned PA6 materials with 5 wt % elastomer content at different temperatures: (a) −40°C, (b) 0°C, and (c) 23°C.

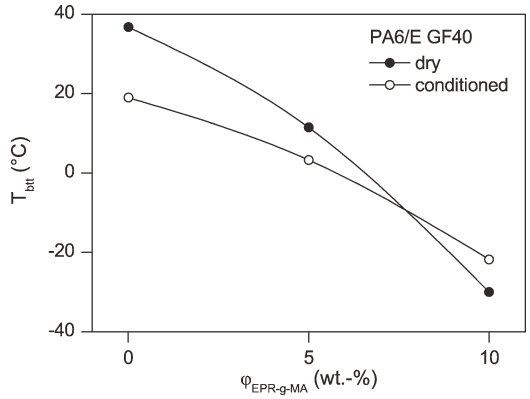

Figure 19. T_{btt} dry and after water absorption.

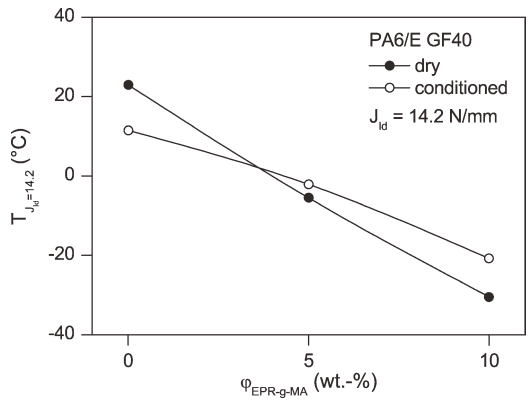

Figure 20. Temperatures of equal J_{Id}.

affects the glass transition temperature and significantly decreases strength and stiffness in the main application temperature range. In return, it was found to be responsible for a significant change in the toughness behavior of these high reinforced materials. Taking into account, elastomer modification the overall positive toughness influence of moisture cannot be assigned unweighted on the behavior of modified high reinforced materials.

Elastomer addition shifts the brittle-to-tough transition towards lower temperatures, but as a specific feature, J_{Id} values proved to be lower in the toughness transition range after water absorption in some cases. This study showed that optimization of toughness in multi-component materials is a complex objective where the fracture mechanical value J_{Id} is an ideal candidate for optimization criterion, as it is energy-driven and takes into account load and deformation influences parallel.

ACKNOWLEDGMENTS

Mrs. C. Becker and Prof. Dr. G. H. Michler from Martin-Luther University Halle-Wittenberg, as well as Dr. Thomas Koch from Vienna University of Technology are gratefully acknowledged for the provision of SEM images. This study was supported by a Max-Buchner research grant of the DECHEMA which is acknowledged just as much. The authors thank the BASF Leuna GmbH for enduring support of this scientific work.

REFERENCES

1. Shojaei, A.; Fereydoon, M. *Mater. Sci. Eng.* **2009,** *506A*, 45.
2. Ping, W. S. Department of Physics and Materials Science, City University of Hongkong, **2008.**
3. Ching, E. C. Y.; Li, R. K. Y.; Tjong, S. C.; Mai, Y.-W. *Polym. Eng. Sci.* **2003,** *43*, 558.
4. Gomina, M.; Pinot, L.; Moreau, R.; Nakache, E. In European Structural Integrity Society; Blackman, B. R. K.; Pavan, A.; Williams, J. G., Eds.; Elsevier, **2003.**
5. Laura, D. M.; Keskkula, H.; Barlow, J. W.; Paul, D. R. *Polymer* **2003,** *44*, 3347.
6. Tjong, S. C.; Xu, S. A.; Mai, Y. W. *Mater. Sci. Eng.* **2003,** *347A*, 338.
7. Laura, D. M.; Keskkula, H.; Barlow, J. W.; Paul, D. R. *Polymer* **2002,** *43*, 4673.
8. Tjong, S. C.; Xu, S.-A.; Kwok-Yiu Li, R.; Mai, Y.-W. *Compos. Sci. Technol.* **2002,** *62*, 2017.
9. Laura, D. M.; Keskkula, H.; Barlow, J. W.; Paul, D. R. *Polymer* **2001,** *42*, 6161.
10. Whan, J.; Paul, C. D. R. *J. Appl. Polym. Sci.* **2001,** *80*, 484.
11. Laura, D. M.; Keskkula, H.; Barlow, J. W.; Paul, D. R. *Polymer* **2000,** *41*, 7165.
12. Nair, S.; Subramaniam, A.; Goettler, L. *J. Mater. Sci.* **1997,** *32*, 5347.
13. Huang, J. J.; Paul, D. R. *Polymer* **2006,** *47*, 3505.
14. Araújo, E. M., Jr.; E. H.; Carvalho, A. J. F. *J. Appl. Polym. Sci.* **2003,** *90*, 2643.
15. Kayano, Y.; Keskkula, H.; Paul, D. R. *Polymer* **1997,** *38*, 1885.
16. Oshinski, A. J.; Keskkula, H.; Paul, D. R. *Polymer* **1996,** *37*, 4919.
17. González-Montiel, A.; Keskkula, H.; Paul, D. R. *Polymer* **1995,** *36*, 4587.
18. González-Montiel, A.; Keskkula, H.; Paul, D. R. *Polymer* **1995,** *36*, 4605.
19. Bethge, I.; Reincke, K.; Seidler, S.; Grellmann, W. In Deformation and Fracture Behavior of Polymers; Grellmann, W.; Seidler, S., Eds.; Springer-Verlag: New York, **2001.**
20. Langer, B.; Seidler, S.; Grellmann, W. In Deformation and Fracture Behavior of Polymers; Grellmann, W.; Seidler, S., Eds.; Springer Verlag: New York, **2001.**
21. Kroll, M.; Langer, B.; Schumacher, S.; Grellmann, W. *J. Appl. Polym. Sci.* **2010,** *116*, 610.
22. Nase, M.; Langer, B.; Schumacher, S.; Grellmann, W. *J. Appl. Polym. Sci.* **2009,** *111*, 2245.
23. International Organization for Standardization. Plastics—Polyamides—Accelerated Conditioning of Test Specimens, **1995.**
24. International Organization for Standardization. Plastics: Determination of Tensile Properties, Part 1: General Principles, **1993.**
25. Grellmann, W.; Seidler, S. Polymer Testing; Carl Hanser Verlag: Munich, **2007.**

26. Grellmann, W.; Seidler, S.; Hesse, W. In Deformation and Fracture Behavior of Polymers; Grellmann, W.; Seidler, S., Eds.; Springer-Verlag: New York, **2001, Chapter A2.2.**
27. International Organization for Standardization.Plastics—Determination of Dynamic Mechanical Properties, Part 1: General Principles,**2001.**
28. Schmack; G.; Vogel; R.; Ussler; L. Strukturbeeinflussung von Polyamiden; Hanser: München, **1994.**
29. Miri, V.; Persyn, O.; Lefebvre, J. M.; Seguela, R. *Eur. Polym. J.* **2009,** *45*, 757.
30. Avramova, N. *J. Appl. Polym. Sci.* **2007,** *106*, 122.
31. Kawagoe, M.; Nabata, M.; Ishisaka, A. *J. Mater. Sci.* **2006,** *41*, 6322.
32. Laredo, E.; Grimau, M.; Sanchez, F.; Bello, A. *Macromolecules* **2003,** *36*, 9840.
33. Bian, X. S.; Ambrosio, L.; Kenny, J. M.; Nicolais, L.; Dibenedetto, A. T. *Polym. Compos.* **1991,** *12*, 333.
34. Hinrichsen, G. *Colloid. Polym. Sci.* **1978,** *256*, 9.
35. Langer, B. Dissertation, Martin-Luther-Universität Halle-Wittenberg, **1997.**
36. Blumenauer, H.; Pusch, G., Technische Bruchmechanik; Deutscher Verlag für Grundstoffindustrie, **2001.**
37. Michler, G. H. Electron Microscopy of Polymers; Springer: Berlin, **2008.**
38. Iwamoto, R.; Murase, H. *J. Polym. Sci. Part B Polym. Phys.* **2003,** *41*, 1722.
39. Pai, C.-C.; Jeng, R.-J.; Grossman, S. J.; Huang, J.-C. *Adv. Polym. Tech.* **1989,** *9*, 157.